Supplementary materials

Materials Characterization

The synthesized samples were analyzed by X-ray diffraction (XRD, PANalytical, Empyrean) with Cu-Kalpha radiation (λ=0.15405 nm), and the phase and crystal structure of the samples were studied. The morphology was measured with a field emission scanning electron microscope (SEM, FEI, Tecnai MLA650F) and the transmission electron microscope (TEM, FEI F20) is used in element distribution analysis. The element and its attribute analysis are determined by X-ray photoelectron spectroscopy (XPS, thermoscientific, ESCALAB 250XI).

Synthesis of $(Fe_{0.75}Ni_{0.25})C_2O_4$ NRs

10 mmol oxalic acid was dissolved in DMAC as solution A. 1.5 mmol of $FeCl_2 \cdot 4H_2O$ and 0.5 mmol of $NiCl_2 \cdot 6H_2O$ was dissolve in 25 mL deionized water as solution B. Slowly add solution B into solution A and stir for 5 min. The above solution was centrifuged with ethanol for three times. The precipitate was dried in an oven at 60 °C and ground to obtain $(Fe_{0.75}Ni_{0.25})C_2O_4$ NRs.

Synthesis of $(Fe_{0.25}Ni_{0.75})C_2O_4$ NRs

10 mmol oxalic acid was dissolved in DMAC as solution A. 0.5 mmol of $FeCl_2 \cdot 4H_2O$ and 1.5mmol of $NiCl_2 \cdot 6H_2O$ was dissolve in 25 mL deionized water as solution B. Slowly add solution B into solution A and stir for 5 min. The above solution was centrifuged with ethanol for three times. The

precipitate was dried in an oven at 60 °C and ground to obtain ($Fe_{0.25}Ni_{0.75}$)C_2O_4 NRs.

Pretreatment of nickel foam(NF)

Cut the NF into affirmative 2*2 mm square. The NF was placed in a 2 mol/L HCl solution for ultrasonic 30min. Then wash with alcohol and deionization. The treated NF was stored in ethanol for use.

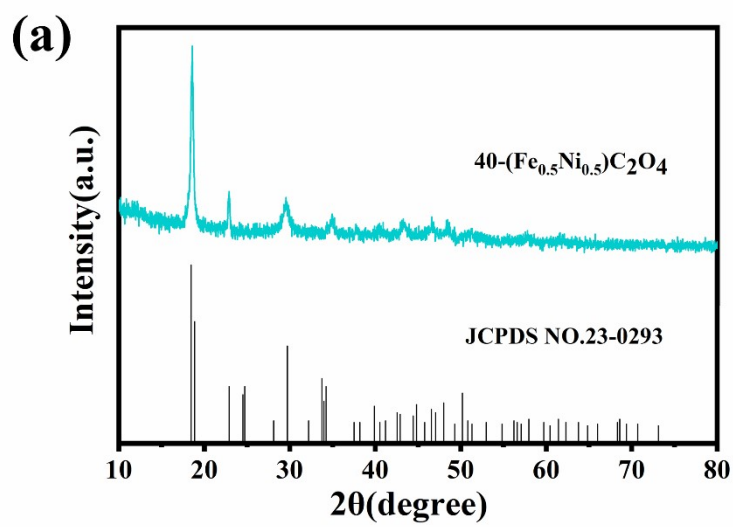

Fig. S1 (a) XRD patterns of 40-($Fe_{0.5}Ni_{0.5}$)C_2O_4.

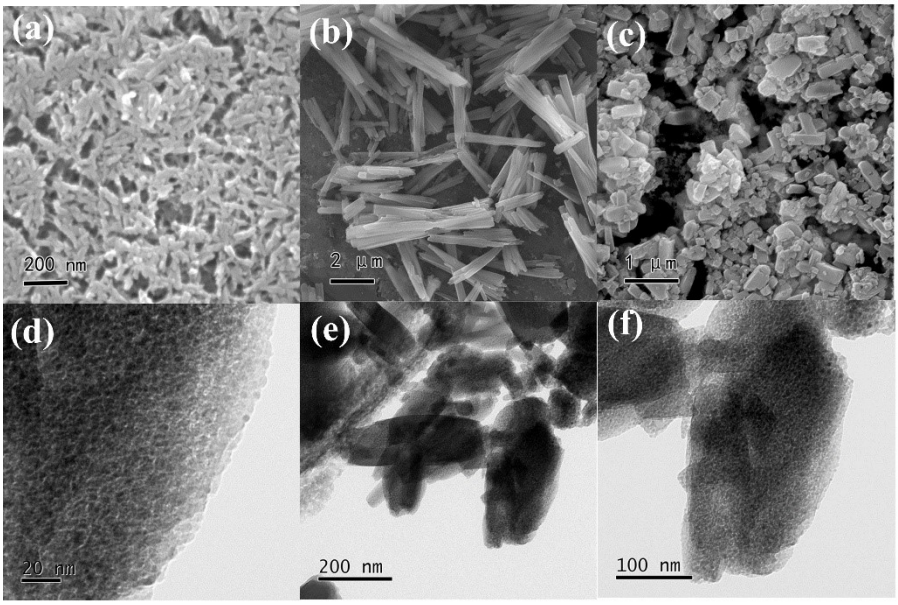

Fig. S2 (a) the SEM images of NiC_2O_4. (b) the SEM images of FeC_2O_4 (c) the SEM images of $(Fe_{0.5}Ni_{0.5})C_2O_4$. (d-f) the TEM images of $(Fe_{0.5}Ni_{0.5})C_2O_4$ low- and high-magnification.

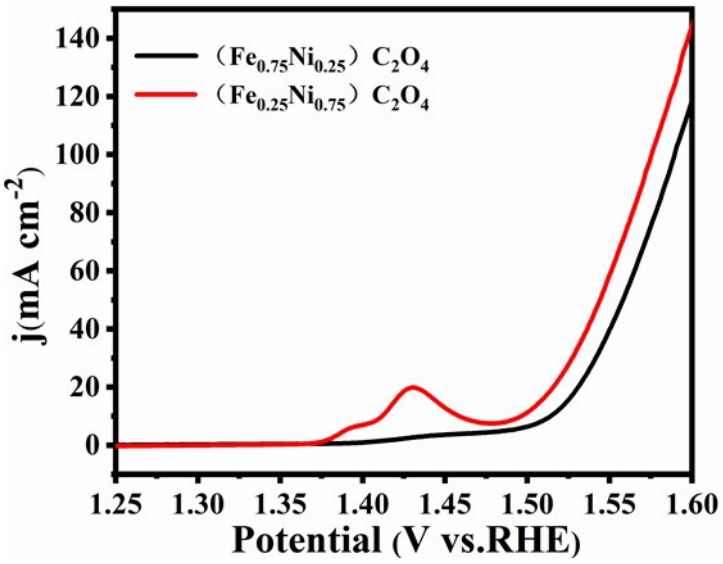

Fig. S3 LSV polarization curves of $(Fe_{0.75}Ni_{0.25})C_2O_4$ and $(Fe_{0.25}Ni_{0.75})C_2O_4$ with 95% iR compensation.

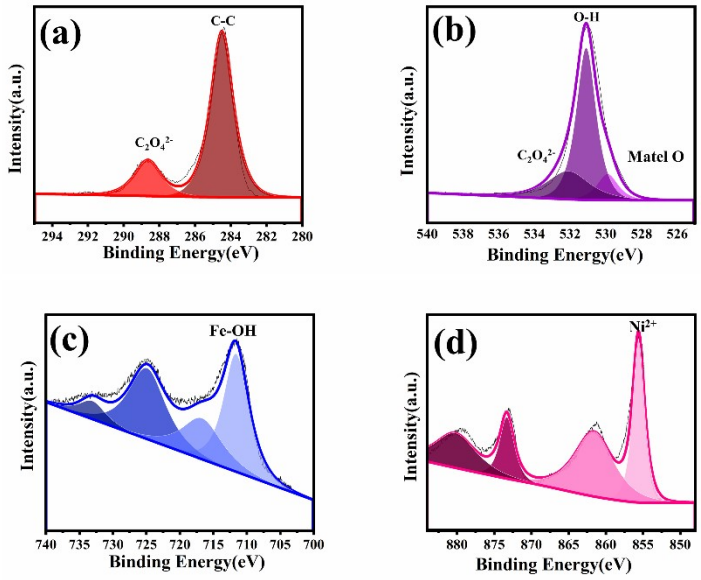

Fig. S4 (a) C_{1s}, (b) O_{1s}, (c) Fe_{2p}, (d) Ni_{2p} XPS spectra of the G-$(Fe_{0.5}Ni_{0.5})C_2O_4$ after the OER measurements.

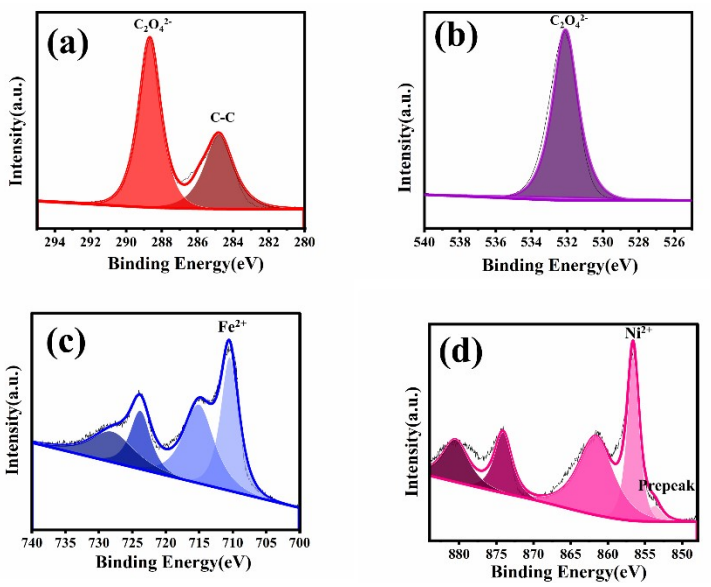

Fig. S5 C_{1s}, (b) O_{1s}, (c) Fe_{2p}, (d) Ni_{2p} XPS spectra of the 40-$(Fe_{0.5}Ni_{0.5})C_2O_4$.

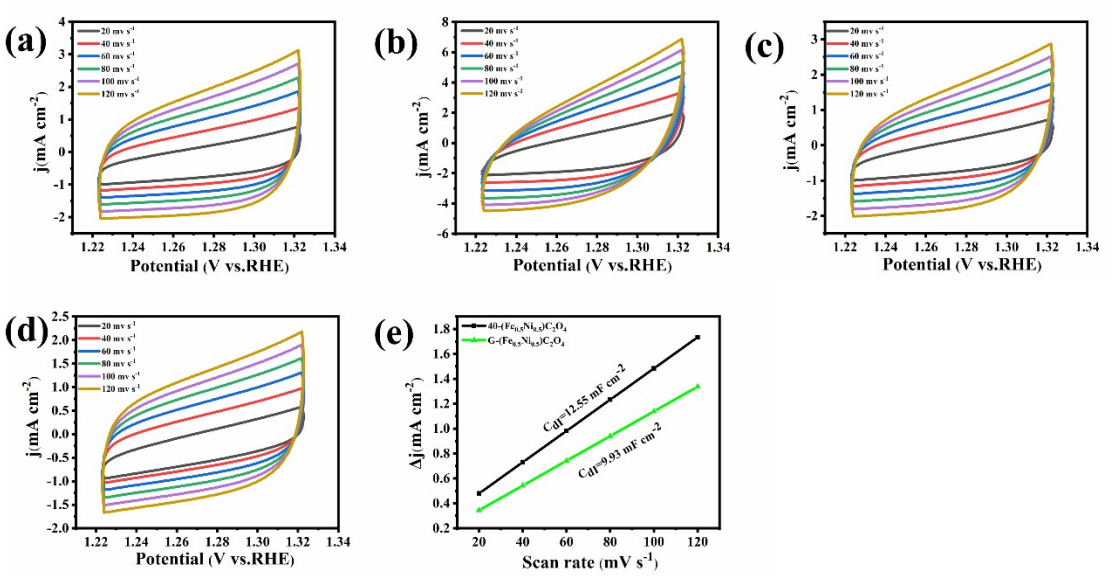

Fig. S6 (a) Cyclic voltammetry curves of FeC_2O_4 in 1M KOH solution with different scan rates. (b) Cyclic voltammetry curves of NiC_2O_4 in 1M KOH solution with different scan rates. (c) Cyclic voltammetry curves of the 40-$(Fe_{0.5}Ni_{0.5})$ C_2O_4 in 1M KOH solution with different scan rates. (d) Cyclic voltammetry curves of G-$(Fe_{0.5}Ni_{0.5})$ C_2O_4 in 1M KOH solution with different scan rates. (e)The relationship between the difference between the anode and cathode current density of all catalysts and the scanning rate.

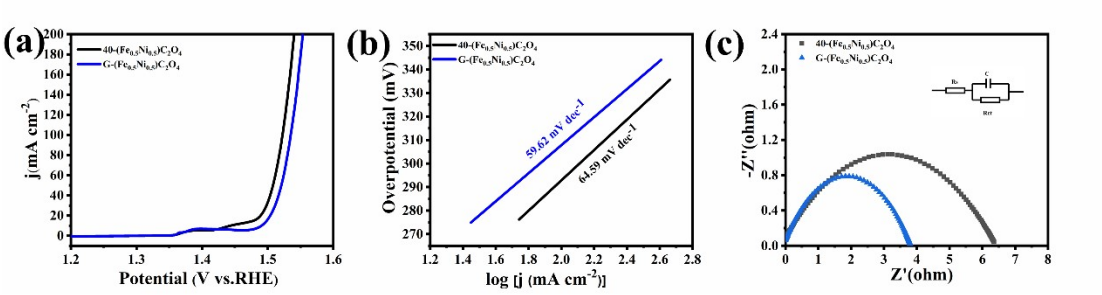

Fig. S7 (a) LSV polarization curves and (b) Tafel plots for OER of 40-$(Fe_{0.5}Ni_{0.5})C_2O_4$ and G-$(Fe_{0.5}Ni_{0.5})C_2O_4$ with 95% iR compensation. (c) Nyquist diagram obtained by electrochemical impedance spectroscopy at 1.6 V vs. RHE 40-$(Fe_{0.5}Ni_{0.5})$ C_2O_4 and G-$(Fe_{0.5}Ni_{0.5})$ C_2O_4 electrocatalysts (inset: equivalent resistance circuit model).

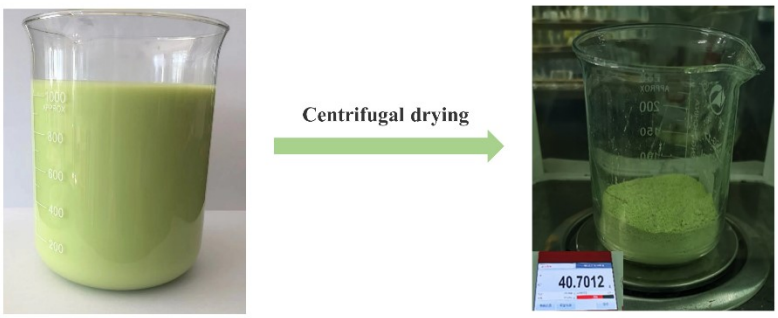

Fig. S8 Schematic diagram of mass production of $(Fe_{0.5}Ni_{0.5})C_2O_4$.

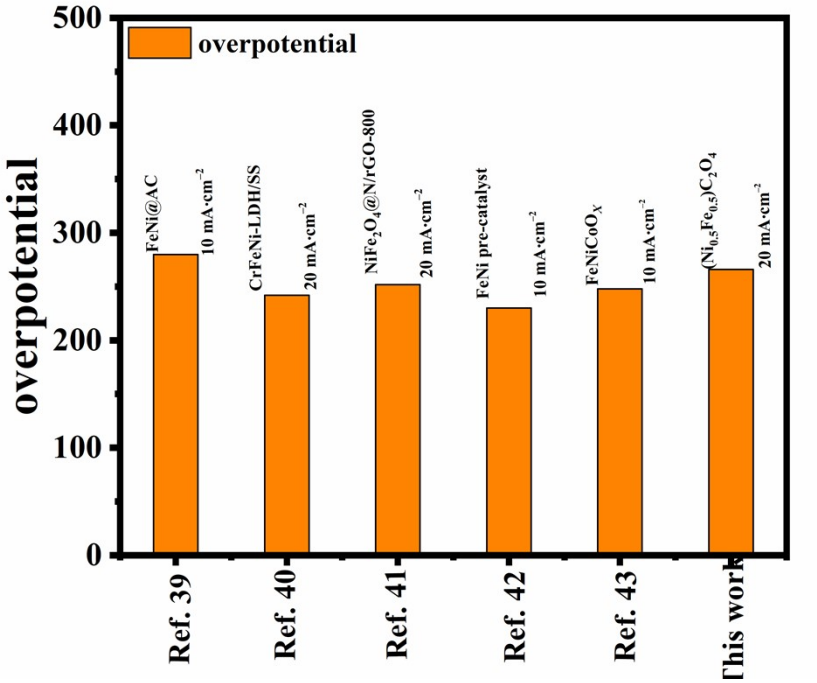

Fig. S9 Comparison of electrochemical activity between $(Fe_{0.5}Ni_{0.5})C_2O_4$ and different reported FeNi compound catalysts.